Available online at www.sciencedirect.com
SCIENCE DIRECT
Journal of Catalysis 238 (2006) 293–300
JOURNAL OF CATALYSIS
www.elsevier.com/locate/jcat

Effect of FeH-zeolite structure and Al-Lewis sites on N_2O decomposition and NO/NO_2-assisted reaction

Dalibor Kaucký, Zdeněk Sobalík, Michael Schwarze, Alena Vondrová, Blanka Wichterlová *

J. Heyrovský Institute of Physical Chemistry, Academy of Sciences of the Czech Republic, Dolejškova 3, CZ-182 23 Prague 8, Czech Republic

Received 20 September 2005; revised 9 December 2005; accepted 16 December 2005

Available online 19 January 2006

Abstract

Fe ions in zeolites of ferrierite and beta structures with Fe content of 0.55 wt% and 0.60 wt% and Fe/Al molar ratios of 0.06 and 0.09, respectively, loaded predominantly in cationic sites, with the zeolites also containing controlled amounts of Al-Lewis sites, were used to analyze the effect of Fe–Fe distances and the simultaneous presence of Fe and Al-Lewis sites on direct N_2O decomposition and NO/NO_2-assisted N_2O decomposition. It was found that shorter Fe–Fe distances in ferrierite result in higher N_2O conversion in direct N_2O decomposition. The presence of Al-Lewis sites in the vicinity of Fe ions also increases the N_2O conversion in direct decomposition on Fe ions. In contrast, NO/NO_2-assisted N_2O decomposition does not discriminate between these effects. It is concluded that the direct N_2O decomposition is structurally site-specific and is controlled by the rate of recombination of oxygen atoms bound to Fe sites, whereas NO/NO_2-assisted N_2O decomposition is controlled by the rate of $NO_2 \rightarrow NO$ conversion occurring on structure-nonspecific Fe sites.

Keywords: N_2O decomposition; NO/NO_2 assistance; Fe-zeolites; Fe-ferrierite; Fe-beta; Fe–Fe distance; Al-Lewis site

1. Introduction

It is well known that specific extra-framework Fe species in ZSM-5 zeolite provide extraordinary activity in reactions involving N_2O, particularly in N_2O decomposition [1,2] and oxidation of benzene to phenol [3–6] and paraffins to olefins and saturated aldehydes [7,8]. The structure of the Fe site active in these oxidations and N_2O decomposition remains a matter of debate, however. Numerous studies have reported the activity and behavior of extra-framework Fe species formed by CVD of $FeCl_3$ [9,10] or from Fe isomorphously substituted in the framework by high-temperature calcination or steaming [11–14]. These materials exhibit a spectrum of Fe species ranging from single Fe ions through Fe-oxo species and to poly-oxo nuclear entities. Both single Fe ions bearing an extralattice oxygen [15] and dinuclear or polynuclear Fe–O–Fe-like species have been suggested as the active sites in N_2O decomposition or hydrocarbon oxidation with N_2O [16–18]. Because the Fe-zeolites exhibit much higher activity per Fe site at low concentrations [19], the specific Fe cations at cationic sites should exhibit extraordinary activity among various types of Fe species detected in Fe-zeolites [19,20]. For this reason, we have focused our attention on the Fe ions exchanged into cationic sites.

N_2O decomposes, yielding gaseous N_2 and O atoms deposited on the Fe active sites at a broad temperature range. Higher temperatures are required to release the O atoms and produce gaseous O_2. It has been proposed that recombination of these O atoms, leading to a molecular O_2, controls the overall rate of N_2O decomposition [21–23].

Besides questions regarding the structure of Fe sites, bonding of atomic oxygens, and conditions of their recombination, there is interest in a general feature of the Fe-based catalysts—enhancement of N_2O decomposition by the presence of NO [24,25]. This property of the NO/N_2O/Fe-zeolite system is highly advantageous for nitrous oxide decomposition in tail gases of nitric acid plants containing $N_2O/NO/NO_2$ mixtures.

The promoting effect of NO in N_2O decomposition was first reported by Kapteijn et al. [24] for Fe-ZSM-5 zeolite and by Turek [25] for Cu-ZSM-5 zeolite. It has been proposed that NO scavenges adsorbed oxygen atoms originating from N_2O de-

* Corresponding author.
E-mail address: wichterl@jh-inst.cas.cz (B. Wichterlová).

0021-9517/$ – see front matter
doi:10.1016/j.jcat.2005.12.017

composition, with consequent formation of NO_2 and recovery of the active site [24–27],

$$N_2O + * \rightarrow N_2 + O* \quad (1)$$

and

$$O* + NO \rightarrow NO_2 + *, \quad (2)$$

leading to a stoichiometric process,

$$N_2O + NO \rightarrow N_2 + NO_2. \quad (3)$$

Kapteijn et al. [28], using multiply time-resolved analysis of reaction kinetics, analyzed the effect of NO on the formation of molecular oxygen in the NO/N_2O/Fe-ZSM-5 system. They suggested that in N_2O decomposition without NO assistance, molecular oxygen is formed by recombination of two oxygen atoms on the catalyst surface or by interaction between another N_2O molecule and an adsorbed oxygen atom to yield molecular oxygen and nitrogen. Similarly, NO can release atomic oxygen from the surface through its oxidation to NO_2 or through N_2O-induced desorption of molecular oxygen from the surface containing deposited oxygen atoms and adsorbed NO_2. Thus two reaction pathways in NO-assisted N_2O decomposition can be considered: one connected with formation of NO_2, and the other with increased formation of O_2. Two alternatives for the enhanced O_2 formation have been suggested: electronic effects of NO adsorbed on sites neighboring the site catalyzing N_2O decomposition [21] and a catalytic cycle involving recombination of oxygen from adsorbed NO_2 and the deposited oxygen atom at Fe sites [25,29]. Although it has been reported that CO or H_2 molecules [25] cause an accelerating effect comparable to NO, an open question remains as to whether the effect of H_2 is distinct up to very low concentration, as for NO [21,26], and whether both effects are accompanied by enhanced formation of O_2.

The positive effect of Fe-ZSM-5 steaming [1,2,11–13] and high-temperature calcination of Fe-FER [30] on its activity in N_2O decomposition have been reported. However, the origin of this effect is still a matter of dispute [31,32]. Pérez-Ramírez et al. [33] reported that steaming of Fe-ZSM-5 containing Fe in the framework changed the nature of Fe species by releasing Fe ions from the framework to extra-framework positions. However, this rearrangement also caused a simultaneous decrease in the concentration of Brönsted sites and formation of some Al-Lewis sites. Although it has been found that the existence of Al-related Lewis sites only (without the presence of trace concentrations of Fe) does not provide activity related to N_2O, some contribution of Al-Lewis sites to the reaction cannot be excluded [6]. Hensen et al. [34] reported increased activity in benzene oxidation to phenol with N_2O with the addition of aluminium to ferri-silicalite (originally without traces of Al), which itself was catalytically inactive. This indicates a possible cooperation of Fe and Al sites. Analogously, we have found that dehydroxylation of Fe-ferrierite accompanied by formation of Al-Lewis sites doubled the deposition of atomic oxygen from N_2O [30].

In general, whether the Fe site needs in its nearest neighborhood the next Fe site for cooperation, and whether such cooperation of sites is also necessary for the NO/NO_2-assisted reaction, remain unclear. If such cooperation is needed, then close (or optimal) distances between two Fe sites in cationic positions might facilitate N_2O decomposition. Therefore, we carried out direct N_2O decomposition and NO/NO_2-assisted N_2O decomposition over FeH-ferrierite and FeH-beta (i.e., over zeolites of differing topologies) with differing distances between Fe site positions.

2. Experimental

Parent NaK-FER zeolite (composition: Si/Al 8.5, Na 0.47 wt%, K 1.98 wt%, Fe impurities 170 ppm) and parent H-*BEA zeolite (composition: Si/Al 12.0, Fe impurities 250 ppm) were purchased from TOSOH and PQ, respectively. The NaK-FER was exchanged with 0.5 M NH_4NO_3 to convert it completely into the NH_4 form. Fe ions were introduced into the zeolites through a reaction of the H- or NH_4-zeolite (dried at increased temperature) with $FeCl_3$ solution in acetylacetone and its subsequent controlled calcination and hydrolysis of the formed iron species in a zeolite by distilled water, as described in detail elsewhere [35,36]. The resulting Fe content was similar in both zeolites:. 0.55 wt% for $FeNH_4$-FER and 0.60 wt% for FeH-*BEA. The corresponding Fe/Al ratio (indicated by numbers in parentheses: Fe(0.06)NH_4-FER and Fe(0.09)H-*BEA) was very low. After dehydration and deammoniation, the zeolites are denoted as FeH-zeolites (Table 1). The well-developed XRD patterns and FTIR spectra in the region of skeletal vibrations (measured by the KBr technique) reflect the highly crystalline regular framework of the both zeolites.

To indicate the presence of Fe ions in cationic sites and to determine the concentrations of Brönsted and Al-Lewis sites, FTIR spectra of OH groups (3800–3100 cm^{-1}) and after sorption of d_3-acetonitrile in the region of C≡N vibrations (2360–2200 cm^{-1}), respectively, were monitored as described previously [37,38]. The spectra were collected on a Nicolet-Magna 550 FTIR spectrometer equipped with a heatable cell connected to a vacuum and gas-supplying system and measured on zeolites in a form of thin, self-supported plates (ca. 5–7 mg/cm^2). The zeolites were firstly dehydrated and deammoniated at 450 °C and then partially dehydroxylated at 700 °C under vacuum for 3 h. Deuterated acetonitrile (13 mbar) was adsorbed at room temperature for 0.5 h, and its physisorbed part was desorbed at the same temperature. d_3-Acetonitrile adsorbed

Table 1
Composition of FeH-zeolites calcined at 450 and 700 °C as determined by chemical analysis and FTIR spectra of adsorbed d_3-acetonitrile

FeH-zeolite	Composition			FTIR	
	Si/Al	Fe (wt%)	Fe/Al	Brönsted sites (mmol/g)	Al-Lewis sites (mmol/g)
FeH-FER 450 °C	8.5	0.55	0.06	0.92	0.36
FeH-FER 700 °C	8.5	0.55	0.06	0.46	0.59
FeH-*BEA 450 °C	12.0	0.60	0.09	0.47	0.35
FeH-*BEA 700 °C	12.0	0.60	0.09	0.24	0.47

on Brönsted and Al-Lewis sites exhibited maxima at 2295 and 2325 cm^{-1}, respectively. The extinction coefficients were $\varepsilon_B = 2.05$ cm/μmol (Brönsted sites) and $\varepsilon_L = 3.60$ cm/μmol (Al-Lewis sites) [38]. Peak deconvolution in the spectra was calculated using Microcal Origin, version 4.1.

Calcination of FeH-zeolites in an oxygen stream at temperature of 450 °C (for 2 h) or a helium stream at 700 °C (for 1 h), followed by calcination in an oxygen stream at 450 °C for 1 h, was done in the reactor before to catalytic experiments. Such treatments provided FeH-zeolites containing, besides Fe sites, predominantly Brönsted acid sites or, in partly dehydroxylated FeH-zeolites, also Al-Lewis sites.

The activity of catalysts in direct N_2O decomposition and NO/NO_2-assisted N_2O decomposition was measured in a quartz through-flow tubular microreactor. The components of the reaction mixtures were fed through mass-flow controllers to the mixing line and diluted there with helium as a carrier gas. The catalyst weight was 0.100 g, and the total flow rate of 100 cm^3/min corresponded to a GHSV of 30,000 h^{-1}. In selected experiments, water vapor, H_2, or O_2 were added into the reactant stream. Water vapor was added by a saturator kept at a constant temperature. Typical concentrations of reactants were 1000 ppm of N_2O, 50–1000 ppm of NO or NO_2, 300–5000 ppm of H_2, 6% O_2 or 1% H_2O (in selected experiments), and the balance helium. The steady-state conversions were reached within 20 min.

The concentrations of reactants and products at the inlet and outlet of the reactor were determined using an on-line connected luminescence NO/NO_2 analyzer (VAMET-CZ), a Hewlett–Packard 5890 II gas chromatograph for separation of N_2 and O_2, and an Advance Otima IR N_2O analyzer. The detection limit for NO, NO_2, and N_2O was 2 ppm.

3. Results

FTIR spectra of the evaluated FeH-zeolites dehydrated at 450 °C in the region of T–O–T perturbed skeletal vibrations (970–860 cm^{-1}, not shown) reflected the introduction of Fe ions by controlled ion exchange into cationic positions. With FeH-FER, two absorption bands, one at 918 cm^{-1} and one of much lower intensity at 936 cm^{-1}, were observed. These T–O–T perturbed vibrations indicate Fe(II) ions in cationic sites [39]. Similar T–O–T vibrations were observed for other divalent cations in cationic sites, that is, Co(II) (915 cm^{-1}), Ni(II) (915 cm^{-1}), Mg(II) (925 cm^{-1}), and Mn(II) (926 cm^{-1}) in metal-exchanged ferrierites [37]. The structure and location of the α- and β-type cationic sites in ferrierite was suggested from the XRD of the framework [40] and coordination of Co(II) and Ni(II)ions at cationic sites of ferrierite and beta [41,42]. Dalconi et al. [43,44] also determined the structure of these sites by synchrotron-powered XRD analysis. Such structure attribution of cationic sites for pentasil-ring zeolites of MOR, FER, MFI, and *BEA topology is already generally accepted in the literature [45,46]. A broad band in the region of skeletal vibrations, centered at 915 cm^{-1}, also indicated perturbation of T–O–T bonds by the Fe(II) ions in the cationic sites of the Fe-beta zeolite [47]. Based on the knowledge on divalent metal ion siting in ferrierite [41] and beta [42] zeolites, we can assume that the β-type sites are populated predominately by Fe(II) cations in these zeolites. The presence of Fe(II) ions in cationic sites in the investigated samples and, in contrast, the absence of a significant amount of Fe oxide phase was also confirmed by Mössbauer spectra of these Fe-zeolites [48]. Moreover, the presence of exchanged Fe(II) ions with open coordination spheres was evidenced by adsorbed d_3-acetonitrile, as given below.

To investigate the effect of the Al site neighboring the Fe site, we analyzed the FeH-zeolites in hydroxylated and dehydroxylated forms. The concentrations of the acidic Brönsted and Al-Lewis sites in the individual zeolites, dehydrated at 450 °C or dehydroxylated at 700 °C, are given in Table 1. The dehydroxylation dramatically changed the population of Brönsted and Al-Lewis acid sites. The concentrations of these sites were obtained from the quantitative analysis of FTIR spectra of O–H vibrations (Figs. 1A and 1C) and those of C≡N vibrations after d_3-acetonitrile adsorption (Figs. 1B and 1D). It appeared that acetonitrile was also adsorbed on Fe(II) ions, which exhibited Lewis-like properties, as followed from an additional band at 2303 cm^{-1} obtained by the spectra deconvolution. Using the sum of the concentration of acidic (Brönsted and Al-Lewis) sites, and taking the Fe content into account, we fit the value of the exchange capacity of the zeolites and found that it was consistent with their chemical composition (Table 1). These results support the predominant location of the Fe(II) ions at exchangable positions.

FeH-FER calcined at 450 °C was active in N_2O decomposition at temperatures above 300 °C (Fig. 2A). Cofeeding of NO together with N_2O substantially increased the conversion in N_2O decomposition and shifted conversion values to lower temperatures. The shift to lower temperature by about 50 °C and decrease in activation energy by ∼30 kJ/mol are nearly consistent with previously reported results for Fe-zeolite-based catalysts [26]. The cofed NO was converted to NO_2; no NO decomposition occurred.

The FeH-*BEA catalyst calcined at 450 °C was much less active in N_2O decomposition (Fig. 2B) compared with FeH-FER. Up to 420 °C, N_2O conversion was <20%. The admixture of NO to the N_2O feed caused a dramatic increase of N_2O conversion on FeH-*BEA in a broad temperature range. The resulting temperature profiles of N_2O conversion coassisted by NO were thus similar for both the FeH-*BEA and FeH-FER zeolites.

The effect of high-temperature (700 °C) dehydroxylation of FeH-zeolites, accompanied by formation of Al-Lewis sites, on the N_2O decomposition activity was significantly different for the individual FeH-zeolites (Fig. 3). The dehydroxylation of FeH-FER considerably increased N_2O conversion; however, if NO was present in the reaction mixture, N_2O conversion was almost identical for FeH-FER calcined at 450 °C and FeH-FER dehydroxylated at 700 °C (Fig. 3A). T he activity of dehydroxylation of FeH-*BEA also improved, but compared with FeH-FER, the effect on N_2O conversion was much lower (Fig. 3B). However, again under cofeeding of NO, both dehydrated and dehydroxylated FeH-*BEA catalysts exhibited high and very similar N_2O decomposition activity. It should be stressed that

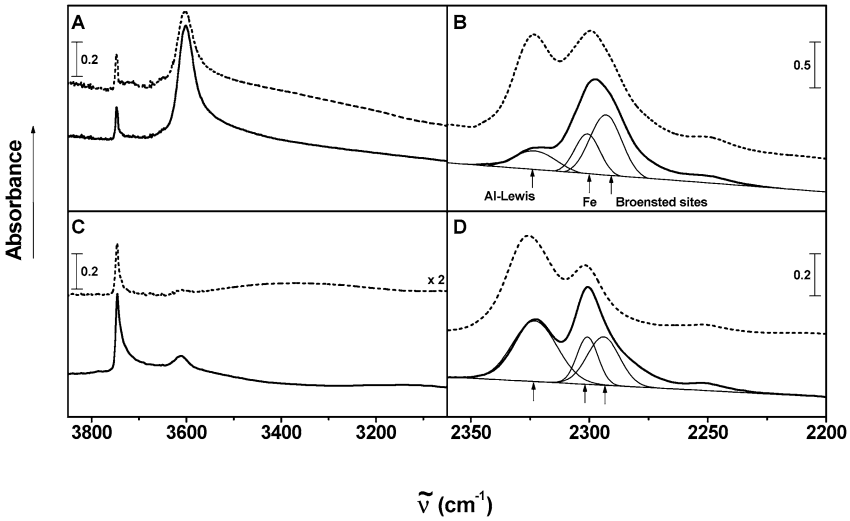

Fig. 1. FTIR spectra of FeH-FER and FeH-*BEA zeolites; dehydrated under vacuum at 450 °C (—) and 700 °C (- - -). FeH-FER in the region of (A) –OH vibrations and (B) C≡N vibrations after sorption of CD_3–C≡N. The bands resulting from the spectra deconvolution are given for illustration; bands at 2325 cm^{-1} represented vibration of CD_3–C≡N adsorbed on Al-Lewis sites and at 2295 cm^{-1} Brönsted sites, at 2303 (from deconvolution procedure) reflected CD_3–C≡N on Fe sites. FeH-*BEA in the region of (C) –OH vibrations and (D) C≡N vibrations after sorption of CD_3–C≡N.

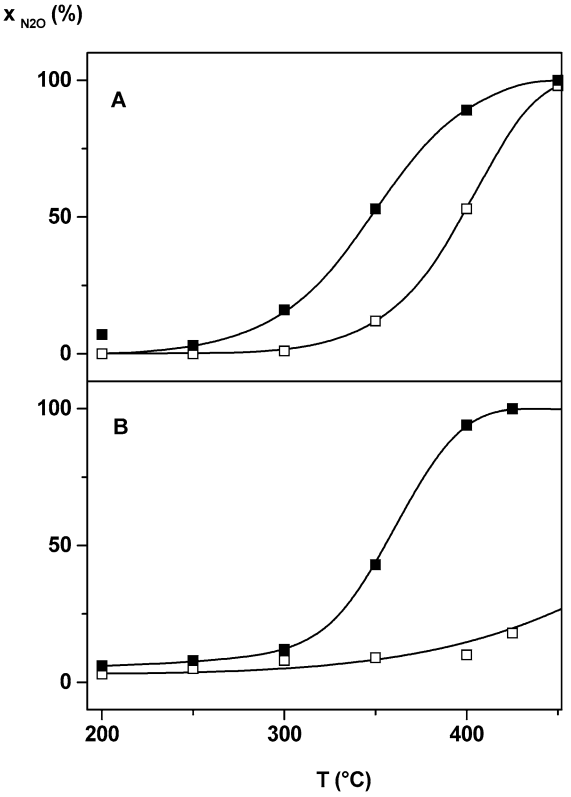

Fig. 2. Conversion of N_2O in its decomposition over FeH-zeolites calcined at 450 °C, if no NO (□) and 500 ppm NO (■) were added into the feed containing 1000 ppm N_2O. (A) FeH-FER; (B) FeH-*BEA.

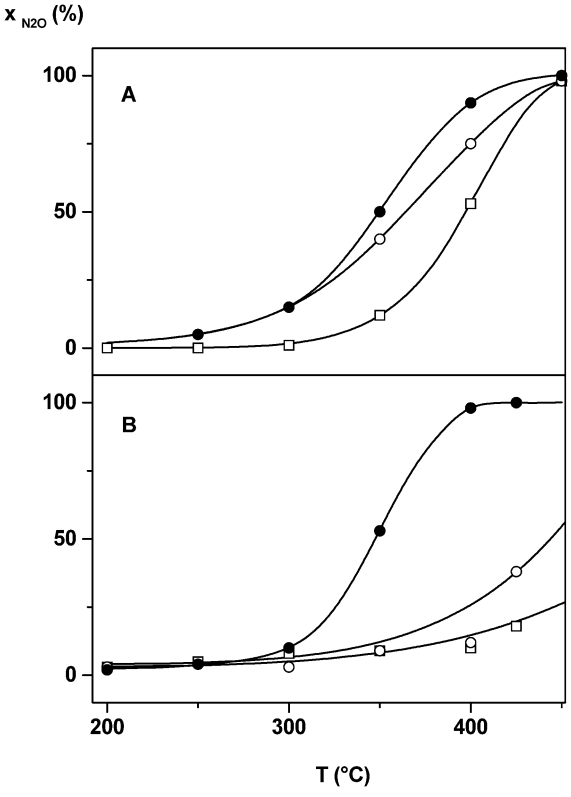

Fig. 3. Conversion of N_2O in direct N_2O decomposition over FeH-zeolites calcined at 450 °C (□), over FeH-zeolites calcined at 700 °C (○) and over FeH-zeolites calcined at 700 °C with the NO added (500 ppm NO) (●) to the feed containing 1000 ppm N_2O. (A) FeH-FER; (B) FeH-*BEA. Reaction conditions the same as for experiments reported in Fig. 2.

with NO-assisted N_2O decomposition, similar results were obtained over FeH-FER and FeH-*BEA zeolites in both their hydroxylated (Figs. 2A and 2B) and dehydroxylated forms (Figs. 3A and 3B).

The effect of 1% water vapor (Table 2) and 6% oxygen (not shown) on N_2O decomposition at 350 and 450 °C with FeH-FER was studied. Although the presence of O_2 did not change the conversion values, 1% H_2O substantially decreased N_2O conversion. But the addition of NO into the feed partly compensated for the negative effect of water vapor. At 350 and 450 °C, N_2O conversion coassisted by NO reached 20 and 80%, respectively.

Table 2
Conversion of N_2O in its decomposition over FeH-FER at 350 and 450 °C depending on the feed composition at dry and wet conditions. The experimental conditions otherwise were the same as in experiments reported in Figs. 2 and 3

Feed			N_2O conversion (%)	
N_2O (ppm)	NO (ppm)	H_2O %	*T* 350 °C	*T* 450 °C
1000	0	0	10	98
1000	0	1	1	8
1000	1000	0	50	100
1000	1000	1	20	80

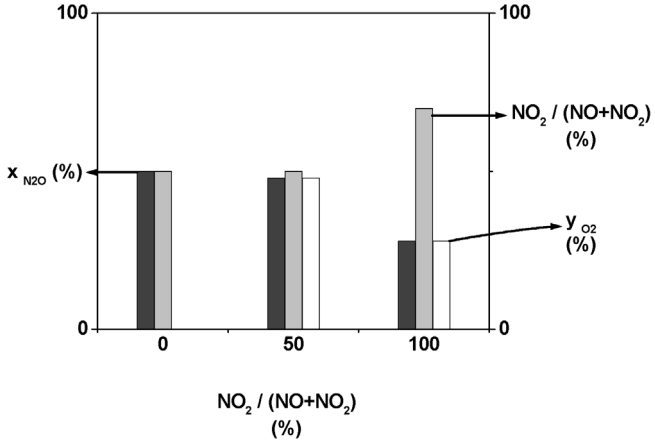

Fig. 4. N_2O decomposition over FeH-FER in the presence of NO, NO_2 or a mixture of NO + NO_2, 350 °C. Conversion of N_2O in dependence on $NO_2/(NO + NO_2)$ ratio in the feed (■). $NO_2/(NO + NO_2)$ ratio in the products in dependence on $NO_2/(NO + NO_2)$ ratio in the feed (□). Yield of O_2 in products in dependence on $NO_2/(NO + NO_2)$ ratio in the feed (□). The part of O_2 originating from $2NO_2 \rightarrow O_2 + 2NO$ was subtracted. Reaction conditions otherwise the same, 1000 ppm N_2O, NO + NO_2 = 1000 ppm.

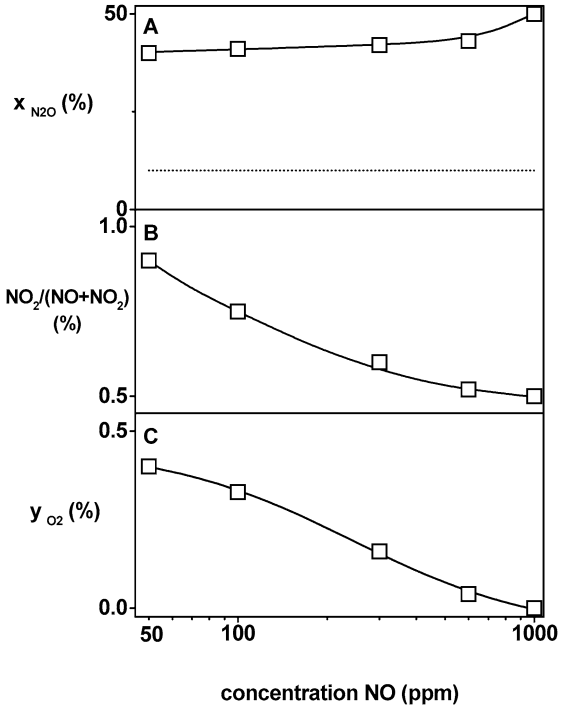

Fig. 5. N_2O decomposition in the presence of NO in feed in dependence on NO concentration FeH-FER, 350 °C. (A) Conversion of N_2O in its NO-assisted decomposition (□) and in its direct decomposition (···); (B) output $NO_2/(NO + NO_2)$ ratio (□); (C) yield of O_2 (□). Reaction conditions otherwise the same, 1000 ppm N_2O.

Besides NO, NO_2 and (NO + NO_2) mixtures also were cofed to the system (Fig. 4). The cofeeding of NO alone or a mixture of NO + NO_2 up to $NO_2/(NO + NO_2) \sim 0.5$ caused practically the same increase in N_2O conversion, by ∼40%. But beyond the $NO_2/(NO + NO_2)$ ratio of ∼0.5, the increasing effect on N_2O conversion was not as high. Cofeeding NO_2 alone increased N_2O conversion to only ∼28%.

The effect of cofeeding the (NO + NO_2) mixtures on oxygen production is also depicted in Fig. 4. When NO alone was cofed, it was converted to NO_2 with a yield of ∼50%, equal to the N_2O conversion value. Thus, all oxygen originating from decomposed N_2O was contained in the formed NO_2, and no O_2 was detected in the products. In contrast, when NO_2 alone was cofed, it was converted to NO, but with a yield of only ∼30%, with an $NO_2/(NO + NO_2)$ output ratio of ∼0.7. At these conditions, the O_2 was also produced from NO_2. Thus, the amount of O_2 originating from NO_2 was subtracted from the total amount of detected O_2; and the residual part of O_2 corresponding to N_2O decomposition is depicted in Fig. 4. The yield of O_2 from N_2O decomposition corresponded well to N_2O conversion. When the mixture of (NO + NO_2) with the $NO_2/(NO + NO_2)$ ratio of ∼0.5 was cofed to N_2O, its ratio remained unchanged during the coassisted N_2O decomposition. As a result, a significant amount of oxygen was detected in the products, practically all originating from accelerated N_2O decomposition. Thus, the maximum production of O_2 during N_2O decomposition was achieved with cofeeding a mixture with a $NO_2/(NO + NO_2)$ ratio of ∼0.5.

The effects of cofed NO in the concentrations of 50–1000 ppm were studied (Fig. 5A). Up to very low NO concentrations, the promoting effect on N_2O conversion remained at the same level (∼40% N_2O conversion with 50 ppm NO in the feed). The yield of produced N_2 closely corresponded with the amount of N_2O converted; thus, oxygen from decomposed N_2O converted NO to NO_2, the yield of which increased with decreasing NO concentration (Fig. 5B). But at low concentrations of added NO, molecular oxygen was formed. The lower the concentration of NO in the feed, the higher the yield of molecular oxygen (Fig. 5C); thus, both nitrogen and oxygen balance closely corresponded with the overall stoichiometry.

To verify the importance of reversibility of interconversions in the NO/NO_2 admixtures, the effect of adding H_2 was evaluated and compared with the effect of NO over FeH-FER. Hydrogen [25,49], like CO [50], has the ability to scavenge O atoms after N_2O decomposition, but undergoes an irreversible $H_2 \rightarrow H_2O$ change. The dependence of augmented N_2O conversion on the concentration of both H_2 and NO is shown in Fig. 6. Clearly, the positive effect of hydrogen on N_2O decomposition decreased with decreasing concentration of added hydrogen, practically in a slopewise manner following the stoichiometry. The effect thus can be considered a first-order reaction with respect to H_2 concentration, in contrast to NO, which exhibited zero-order behavior.

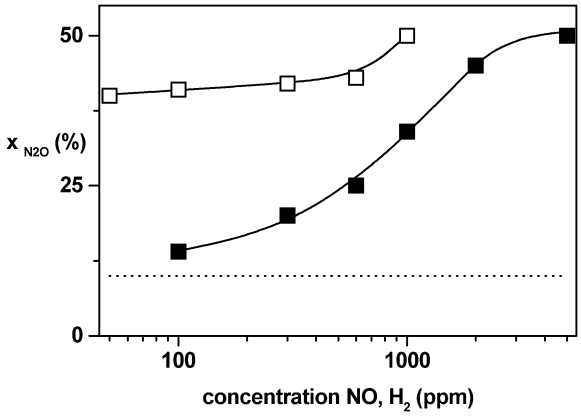

Fig. 6. N_2O conversion in the presence of NO or H_2 in dependence on NO or H_2 concentration FeH-FER, 350 °C, with added NO (□) or H_2 (■). The conversion of N_2O in its direct decomposition (···). Reaction conditions otherwise the same, 1000 ppm N_2O.

However, a further increase in NO or H_2 concentration did not result in an increased N_2O conversion above ca. ∼55% at 350 °C over FeH-FER. Even when H_2 and NO were added together with N_2O, N_2O conversion > ca. ∼55% was not achieved, due to the fact that NO was not converted in the system if hydrogen in a comparable concentration was added. The effect exhibited a saturation level behavior, as was also found on Fe-ZSM-5 [26].

4. Discussion

N_2O decomposition and its acceleration by NO/NO_2 was studied over two FeH-zeolites differing in terms of topology and density of the framework and also by the presence or absence of Al-Lewis sites. Fe ion exchange of zeolites through a method using $FeCl_3$ in acetylacetone with controlled heating [35,36] led to a predominant introduction of Fe(II) ions into cationic sites. This is supported by the low level of the Fe ion exchange (Fe/Al 0.06 and 0.09), IR spectra of adsorbed d_3-acetonitrile evidencing the presence of single Fe(II) sites with open coordination spheres (see the band at 2303 cm^{-1} in Figs. 1B and 1D), and bands of perturbation of the framework T–O–T bonds in the 915–936 cm^{-1} region. The β-type sites have been shown to be preferentially occupied by divalent cations with FER and *BEA structures [41,42]. Supposing that the Fe(II) ions occupy similar sites as the other divalent cations in FeH-FER and FeH-*BEA, their sites could be used for estimating intercation distances. The β-type sites are formed by six-member rings located on the walls of the eight-member ring channel of FER and the 12-member ring channel of *BEA structure [41,42]. Because the beta zeolite structure has a lower framework density than ferrierite, larger distances between the cations in cationic sites can be expected.

The distances between the Fe(II) ions were estimated as follows. For the Fe(II) sites, the estimated structurally allowed distances between the individual Fe(II) ions can be considered the distances between the centers of the nearest cationic sites, assuming that the individual Fe(II) ions lie near the center of the corresponding ring. The distances between the neighboring β-type sites are estimated to be substantially shorter in FER than in *BEA (6.1 Å vs. 7.5 Å, respectively). Although the Fe(II) ions in the zeolites may not be located exactly in the center of the ring forming the β-site, nevertheless, the substantial differences in the Fe–Fe distances in FER and *BEA encourage us to consider the effect of "close" and "distant" Fe(II) ions in Fe-zeolites on N_2O decomposition activity.

If the Fe ion in the cationic site is expected to cooperate with the next Fe ion, then the short distance might increase the probability of cooperation between these close Fe active sites. In contrast, with the FeH-zeolite of *BEA, the nearest Fe ions in β-type sites farther apart, and thus their cooperation might be less efficient. Such a model can assume that the Fe ion bearing an oxygen atom (after N_2O decomposition) should adjoin a nearby Fe site bearing another oxygen atom needed for their recombination to molecular oxygen. This model follows from the experimentally found N_2O conversion values (see Fig. 2B), which were much higher for FeH-FER than for FeH-*BEA. This finding also encourages us to suggest that the formation of molecular oxygen proceeds through recombination of the oxygen atoms and not through interaction of another N_2O molecule with the atomic oxygen bound to the Fe ion. The former mechanism of molecular oxygen formation from N_2O has also been suggested by Kiwi-Minsker et al. [51,52].

The IR vibrations of T–O–T bonds perturbed due to bonding of Fe(II) ions in the β-sites were similar for zeolites dehydrated at 450 °C and those dehydroxylated at 700 °C. In addition, Mössbauer spectra of Fe ions in these zeolites indicated no significant change in the coordination of Fe(II) ions after zeolite dehydroxylation [48]. It follows that treatment of FeH-zeolites at high temperature (700 °C) did not significantly change the structure and distribution of Fe(II) ions. But high-temperature treatment causes partial dehydroxylation and formation of a considerable concentration of Al-Lewis sites from Brönsted sites (see Table 1). Thus, the presence of Al-Lewis sites along with Fe sites can account for the significantly increased N_2O conversion observed in both FeH-FER and FeH-*BEA. Because N_2O decomposition forming molecular nitrogen and deposited oxygen does not proceed on Al-Lewis sites themselves, the enhanced rate of N_2O decomposition to molecular nitrogen and oxygen cannot stem from the enhanced recombination of neighboring oxygen atoms. We suggest that neighboring electron acceptor Al-sites may affect the properties of the Fe ion and/or its surrounding by an electronic effect, causing enhanced recombination of oxygen atoms from the Fe sites.

In contrast to direct N_2O decomposition, the activity of FeH-zeolites in N_2O decomposition assisted by NO/NO_2 does not depend on the Fe–Fe distances (hosting zeolite structure) or on the presence of Al-Lewis sites. This implies that mutual cooperation between the Fe sites or between Fe and Al-Lewis sites is not necessary in the presence of NO/NO_2. Accordingly, the high N_2O conversion in NO/NO_2-assisted N_2O decomposition, independent of the Fe–Fe distances and the presence of Al-Lewis sites, confirms that the mechanisms of N_2O decomposition [26] are quite different for direct and NO/NO_2-assisted N_2O decomposition.

The actual concentration of NO available to assist N_2O decomposition is in fact very low. In all likelihood, each NO molecule fed or formed from NO_2 is immediately consumed in a catalytic cycle of N_2O decomposition. The presence of these two catalytic cycles leads to apparent concentrations of NO_2 over equilibrium [26]. In such a situation, the overall rate could be limited by the rate of conversion of NO_2 to NO.

Another interesting finding is that an increase in NO concentration above a NO/N_2O ratio of $\sim$1 does not further accelerate N_2O decomposition, indicating a saturation behavior, as has been found on Fe-ZSM-5 [26]. This effect can be explained by considering that the overall reaction rate in the presence of higher than stoichiometric amounts of NO is already controlled by the $N_2O \rightarrow N_2 + O$ reaction step, which cannot be sped up any further by NO.

5. Conclusions

From the results of our work, we can draw the following conclusions:

- Direct N_2O decomposition seems to be controlled by the rate of recombination of two deposited O atoms, which requires the cooperation of two close Fe sites. Thus, shorter distances between the Fe cations, such as in FeH-FER compared with FeH-*BEA, enhance the rate of N_2O decomposition. The presence of electron-acceptor Al-Lewis sites in the vicinity of the Fe sites enhances the rate of N_2O decomposition as well, likely through an electronic effect.
- In contrast, NO-assisted N_2O decomposition is not sensitive to the structure-specific Fe active sites. The rate of NO-assisted N_2O decomposition is controlled by the rate of $NO_2 \rightarrow NO$ transformation. It follows that N_2O decomposition under such conditions does not require structure-specific sites, as are required for recombination of the adsorbed oxygen atoms.
- The enhanced O_2 formation during N_2O decomposition accelerated by NO/NO_2 occurs especially at low concentrations or specific NO/NO_2 ratios in the feed, where the rate appears to be controlled by $NO \leftrightarrow NO_2$ interconversion. At high NO_x concentrations (exceeding N_2O concentrations), the rate of N_2O decomposition appears to be controlled by the $N_2O \rightarrow N_2 + O$ process, which cannot be sped up by NO.

Acknowledgments

The authors thank P. Štěpánek for helping with the experiments and Z. Tvarůžková for providing FTIR measurements. D.K. thanks to the Grant Agency of the Czech Republic (project 104/02/D124) for financial support; other authors acknowledge support of the Academy of Sciences of CR under the project 1ET400400413.

References

[1] J. Pérez-Ramírez, F. Kapteijn, G. Mul, J.A. Moulijn, Catal. Commun. 3 (2002) 19.
[2] J. Pérez-Ramírez, F. Kapteijn, G. Mul, X. Xu, J.A. Moulijn, Catal. Today 76 (2002) 55.
[3] G.I. Panov, G.A. Sheveleva, A.S. Kharitonov, V.N. Romannikov, L.A. Vostrikova, Appl. Catal. A: Gen. 82 (1992) 31.
[4] G.I. Panov, A.S. Kharitonov, V.I. Sobolev, Appl. Catal. A: Gen. 98 (1993) 1.
[5] A.S. Kharitonov, G.A. Sheveleva, G.I. Panov, V.I. Sobolev, Y.A. Paukshtis, V.N. Romannikov, Appl. Catal. A: Gen. 98 (1993) 33.
[6] P. Kubánek, B. Wichterlová, Z. Sobalík, J. Catal. 211 (2002) 109.
[7] J. Pérez-Ramírez, A. Gallardo-Llamas, J. Catal. 223 (2) (2004) 382; J. Pérez-Ramírez, A. Gallardo-Llamas, Appl. Catal. A: Gen. 279 (2005) 117.
[8] R. Bulánek, B. Wichterlová, K. Novoveská, V. Kreibich, Appl. Catal. A: Gen. 264 (2004) 13.
[9] P. Marturano, L. Drozdová, A. Kogelbauer, R. Prins, J. Catal. 192 (2000) 236.
[10] P. Marturano, L. Drozdová, G.D. Pirngruber, A. Kogelbauer, R. Prins, Phys. Chem. Chem. Phys. 3 (2001) 5585.
[11] S. Bordiga, R. Buzzoni, F. Geobaldo, C. Lamberti, E. Giamello, A. Zecchina, G. Leofanti, G. Petrini, G. Tozzola, G. Vlaic, J. Catal. 158 (1996) 486.
[12] G. Berlier, G. Spoto, S. Bordiga, G. Ricchiardi, P. Fisicaro, A. Zecchina, I. Rossetti, E. Selli, L. Forni, E. Giamello, C. Lamberti, J. Catal. 208 (2002) 64.
[13] A.M. Ferretti, C. Oliva, L. Forni, G. Berlier, A. Zecchina, C. Lamberti, J. Catal. 208 (2002) 83.
[14] G. Berlier, A. Zecchina, G. Spoto, G. Ricchiardi, S. Bordiga, C. Lamberti, J. Catal. 215 (2003) 264.
[15] A. Heyden, B. Peters, A.T. Bell, F.J. Keil, J. Phys. Chem. B 109 (2005) 1857.
[16] K.A. Dubkov, N.S. Ovanesyan, A.A. Shteinman, E.V. Starokon, G.I. Panov, J. Catal. 207 (2002) 341.
[17] G.I. Panov, A.K. Uriarte, M.A. Rodkin, V.I. Sobolev, Catal. Today 41 (1998) 365.
[18] M.J. Filatov, A.G. Pelmenschikov, G.M. Zhidomirov, J. Mol. Catal. 80 (1993) 243.
[19] G.D. Pirngruber, P.K. Roy, N. Weiher, J. Phys. Chem. B 108 (2004) 13746.
[20] L. Čapek, V. Kreibich, J. Dědeček, T. Grygar, B. Wichterlová, Z. Sobalík, J.A. Martens, R. Brosius, V. Tokarová, Microporous Mesoporous Mater. 80 (2005) 279.
[21] G. Mul, J. Pérez-Ramírez, F. Kapteijn, J.A. Moulijn, Catal. Lett. 77 (2001) 7.
[22] G.D. Pirngruber, J. Catal. 219 (2003) 456.
[23] C. Sang, B.H. Kim, C.R.F. Lund, J. Phys. Chem. B 109 (2005) 2295.
[24] F. Kapteijn, J. Rodrigues-Mirasol, J.A. Moulijn, Appl. Catal. B: Environ. 9 (1996) 25.
[25] T. Turek, J. Catal. 174 (1998) 98.
[26] J. Pérez-Ramírez, F. Kapteijn, G. Mul, J.A. Moulijn, J. Catal. 208 (2002) 211.
[27] J. Pérez-Ramírez, J. Catal. 227 (2004) 512.
[28] F. Kapteijn, G. Marbán, J. Rodrigues-Mirasol, J.A. Moulijn, J. Catal. 167 (1997) 256.
[29] M. Kögel, B.M. Abu-Zeid, M. Schwefer, T. Turek, Catal. Commun. 2 (2001) 273.
[30] J. Nováková, M. Schwarze, Z. Tvarůžková, Z. Sobalík, Catal. Lett. 98 (2004) 123.
[31] J.A.Z. Pieterse, S. Booneveld, R.W. van den Brink, Appl. Catal. B: Environ. 51 (2004) 215.
[32] J. Pérez-Ramírez, F. Kapteijn, Appl. Catal. B: Environ. 47 (2004) 177.
[33] J. Pérez-Ramírez, F. Kapteijn, A. Brückner, J. Catal. 218 (2003) 234.
[34] E.J.M. Hensen, Q. Zhu, R.A. van Santen, J. Catal. 220 (2003) 260.
[35] Z. Sobalík, J.E. Šponer, Z. Tvarůžková, A. Vondrová, S. Kuriyavar, B. Wichterlová, Stud. Surf. Sci. Catal. 135 (2001) 136.

[36] Z. Sobalík, B. Wichterlová, M. Markvart, Z. Tvarůžková, CZ Patent 293 917 (2004).
[37] Z. Sobalík, Z. Tvarůžková, B. Wichterlová, J. Phys. Chem. B 102 (1998) 1077.
[38] B. Wichterlová, Z. Tvarůžková, Z. Sobalík, P. Sarv, Microporous Mesoporous Mater. 24 (1998) 223.
[39] Z. Sobalík, Z. Tvarůžková, B. Wichterlová, Microporous Mesoporous Mater. 25 (1998) 225.
[40] W.J. Mortier, Compilation of Extra Framework Sites in Zeolites, Butterworth & Co, Guildford, 1982.
[41] J. Dědeček, D. Kaucký, B. Wichterlová, Microporous Mesoporous Mater. 31 (1999) 75.
[42] J. Dědeček, L. Čapek, D. Kaucký, Z. Sobalík, B. Wichterlová, J. Catal. 211 (2002) 198.
[43] M.C. Dalconi, G. Cruciani, A. Alberti, P. Ciambelli, M.T. Rapacciuolo, Microporous Mesoporous Mater. 39 (2000) 423.
[44] M.C. Dalconi, A. Alberti, G. Cruciani, P. Ciambelli, E. Fonda, Microporous Mesoporous Mater. 62 (2003) 191.
[45] N.A. Kachurovskaya, G.M. Zhidomirov, R.A. van Santen, J. Phys. Chem. B 108 (2004) 5944.
[46] L.J. Lobree, I.-Ch. Hwang, J.A. Reimer, A.T. Bell, J. Catal. 186 (1999) 242.
[47] Z. Sobalík, J.E. Šponer, B. Wichterlová, Stud. Surf. Sci. Catal. 130 (2000) 1463;
A. Corma et al. (Eds.), Proceedings of the 12th ICC, Granada, Spain, July 9–14, 2000.
[48] M. Schwarze, Z. Sobalík et al., in preparation.
[49] K.A. Dubkov, E.V. Starokon, E.A. Paukshtis, A.M. Volodin, G.I. Panov, Kinet. Catal. 45 (2004) 202.
[50] M.N. Debbagh Boutarbouch, J.M. García Cortés, M. Soussi El Begrani, C. Salinas Martínez de Lecea, J. Pérez-Ramírez, Appl. Catal. B: Environ. 54 (2004) 115.
[51] L. Kiwi-Minsker, D.A. Bulushev, A. Renken, J. Catal. 219 (2003) 273.
[52] D.A. Bulushev, L. Kiwi-Minsker, A. Renken, J. Catal. 222 (2004) 389.